Unravelling the metal uptake process in mosses: comparison of aquatic and terrestrial species as air pollution biomonitors

García-Seoane, R.[+1], Antelo, J.[+2], Fiol, S.[3], Fernández, J.A.[4], Aboal, J.R.[4]

[1]*Instituto Español de Oceanografía (IEO-CSIC), Centro Oceanográfico de A Coruña, 15001, A Coruña, Spain*

[2]*CRETUS. Department of Soil Science and Agricultural Chemistry, Universidade de Santiago de Compostela, 15782, Santiago de Compostela, Spain*

[3]*CRETUS. Department of Physical Chemistry, Universidade de Santiago de Compostela, 15782, Santiago de Compostela, Spain*

[4]*CRETUS. Department of Functional Biology, Ecology Unit, Universidade de Santiago de Compostela, 15782, Santiago de Compostela, Spain*

[+]These authors contributed equally to this work.

*Corresponding author: García-Seoane, R.

E-mail address: rita.garcia@ieo.csic.es/ritagarciaseoane@gmail.com

Abstract

Transplanted mosses have been widely shown to be excellent tools for biomonitoring air pollution; however, it is not clear how the functional groups present on their surfaces affect the uptake of metal cations. In the present study, we examined differences in trace metal accumulation in two terrestrial and one aquatic moss species, and investigated whether the differences depended on their physico-chemical characteristics. In the laboratory, we determined C, N and H contents in their tissues and obtained the ATR-FTIR spectra (to identify the presence of functional groups). We also conducted surface acid-base titrations and metal adsorption assays with Cd, Cu and Pb. In the field, we exposed transplants of each

species near different air-polluting industries, and determined the mosses enrichment of Al, Cd, Co, Cr, Cu, Fe, Ni, Pb and V. Laboratory results demonstrated higher metal uptake capacity in the terrestrial mosses *Sphagnum palustre* and *Pseudoscleropodium purum*, compared to that in the aquatic moss *Fontinalis antipyretica*, which can be attributed to a greater abundance of acidic functional groups (i.e. negatively charged binding sites) on the surface of the terrestrial mosses. The affinity of moss for certain elements depends on the abundance and nature of surface functional groups. Accordingly, the metal concentrations generally reached higher levels in *S. palustre* transplants compared to the other species, except for the uptake of Hg, which was higher in *F. antipyretica*. However, the findings also suggest an interaction between the type of environment (terrestrial or aquatic) and the moss characteristics that may influence the abovementioned trend. Thus, irrespective of the physico-chemical characteristics, metal uptake varied depending on the environment of origin of the mosses "i.e. atmospheric or aquatic". In other words, the findings suggest that species that accumulate more metals in terrestrial environments will accumulate lower amounts of metals in aquatic environments and vice versa.

Keywords: active biomonitoring, air pollution, moss bags, *Pseudoscleropodium purum*, *Sphagnum palustre, Fontinalis antipyretica*

1. Introduction

Air pollution in urban and industrial areas constitutes a major environmental and human health problem (Shahid et al., 2017; Xue et al., 2022). Despite technological advances in air pollution monitoring, biomonitoring remains an excellent option for evaluating atmospheric deposition of pollutants, largely due to its low cost and the possibility of generating high spatial resolution maps. Thus, in recent years, biomonitoring with mosses has made it possible to detect previously unknown sources of pollution by certain elements (Donovan et al., 2016) associated with important environmental health problems (Comess et al., 2021). The spatial resolution that can be obtained makes these biomonitors particularly attractive for use in urban environments, especially in the form of transplants (i.e. moss bags).

Maximising the uptake capacity of the biomonitor used in the moss bags transplant technique is essential for optimizing this methodology. Thus, higher concentrations of pollutants can be retained in the moss tissues, which facilitates their analysis and allows for shorter exposure times. The exposure periods required when using moss bags as air biomonitors are currently very long (usually 4–12 weeks; Ares et al., 2012, 2014; Capozzi et al., 2016), which detracts from the temporal resolution of the technique. To further reduce the exposure period and improve the temporal resolution, different approaches have been evaluated in recent years (Ares et al., 2012): i) maximising the carrying capacity by pre-exposure washing (e.g. Di Palma et al., 2016); ii) using devitalisation treatments (Giordano et al., 2009); and iii) selecting more efficient species as biomonitors (e.g. González and Pokrovsky, 2014). Behind these methodological issues lies, perhaps more importantly, the generation of knowledge about moss pollutant uptake processes. Although hundreds of studies have been conducted using mosses as biomonitors, we are still far from having a good understanding of the processes involved.

In relation to selection of the particular species used as biomonitors, one of the most important criteria is that the structural and physico-chemical characteristics of the moss allow

efficient uptake of elements (Ares et al., 2012). Whereas the thallus morphology determines the capacity to accumulate particles and associated trace metals (Varela et al., 2023), the cation exchange capacity (CEC) -which in turn depends on the specific surface area- and the nature and density of functional groups present on the moss surface affect the adsorption and uptake of cations (Varela et al., 2023).

Recent studies have indicated that *Sphagnum* sp., rather than other terrestrial moss species such as e.g. *Hypnum* sp., *Pseudoscleropodium purum* and *Brachytecium rutabulum*, was the best candidate of those tested for use in the moss bag technique (except for monitoring Hg) based on its physico-chemical characteristics (González and Pokrovsky, 2014) relative to those of *P. purum* (Ares et al., 2014, Capozzi et al. 2017). In recent studies (Debén et al., 2016, 2017) the suitability of terrestrial *Sphagnum* sp. for biomonitoring aquatic ecosystems was tested and its performance was compared with that of *Fontinalis antipyretica*, the aquatic moss species most commonly used for biomonitoring aquatic systems. Surprisingly, the bioaccumulated concentrations of most of the elements studied (e.g. Al, Fe, Hg, Pb, Zn, etc.) were higher in the aquatic moss than in the terrestrial moss. Hence, there are two possible explanations for the higher loadings observed in *F. antipyretica*: i) the importance of the accumulation of adhered particles in the uptake process, with *F. antipyretica* being more efficient in this respect due to its morphological characteristics, ii) a higher density of functional groups responsible for the biosorption of these elements in *F. antipyretica*, and iii) the environment of origin of the mosses (atmospheric or aquatic) prior to its use as a biomonitor.

Based on preliminary findings, we hypothesize that higher metal loads will be reached in *F. antipyretica* than in *Sphagnum* sp. and *P. purum*, unless there is a first-order interaction between species and environment (i.e. atmospheric or aquatic) that affects the loads. To test this hypothesis, we compared the efficiency as biomonitors of metal pollution of the aquatic moss *F. antipyretica* with that of species of the genus *Sphagnum* (as previously mentioned, the best candidate within the terrestrial mosses) and *P. purum* within the same environment of

98 exposure, i.e. atmospheric. For this purpose, mosses should first be devitalized, as metal
99 loading is affected by moss metabolism. As demonstrated for both terrestrial and aquatic
100 mosses, devitalization results in a constant level of retention, as the retention capacity is
101 mainly due to uptake processes that are independent of the moss vitality (Adamo et al., 2007;
102 Giordano et al., 2009; Debén et al., 2016).
103 The main objective of the present study was to ascertain whether the aquatic moss *F.*
104 *antipyretica*, commonly used to biomonitor inland water quality, could be used to biomonitor
105 air pollution. We also evaluated whether the aquatic moss produced better results in
106 atmospheric environment than two terrestrial mosses commonly used as air biomonitors, i.e.
107 *S. palustre* and *P. purum*. Further, the study aimed to verify the possible effect of a first-order
108 interaction between species and environment (atmospheric or aquatic) on metal uptake
109 (related to particle adhesion and metal cation adsorption processes). For this purpose, a field
110 experiment was carried out to compare the accumulation capacity of several potentially toxic
111 elements in the aquatic moss *F. antipyretica* and the terrestrial mosses *S. palustre* and *P. purum.*
112 In addition, a detailed metal binding study was conducted in the laboratory with Cd, Cu and
113 Pb as target trace metals, in order to explore the mechanisms underlying metal adsorption
114 on the surface of the three mosses. These elements were selected because they exhibit high
115 affinity for reactive environmental (bio)surfaces (Davis et al., 2003; He and Chen, 2014;
116 Priyadarshanee and Das, 2021), and good correlations between atmospheric deposition and
117 moss metal content have also been obtained (Aboal et al., 2010).

118 **2. Material and methods**

119 *2.1. Moss samples*

120 The species selected for the study were the terrestrial moss *Pseudoscleropodium purum* (Hedw.)
121 M. Fleisch., the peat moss *Sphagnum palustre* L., and the aquatic moss *Fontinalis antipyretica*
122 Hedw. Samples of *P. purum* and *F. antipyretica* were collected from unpolluted sites in Galicia
123 (NW Spain), far from known sources of pollution. Briefly, *P. purum* was collected in a rural

124 area with low pollution levels (X = 549690; Y = 4733662; UTM 29 N WGS84) and far from
125 main roads and population centres (Carvajal et al., 2010), whereas *F. antipyretica* was collected
126 from a small unpolluted stream (X = 530461; Y = 4740421; UTM 29 N WGS84). The species
127 *S. palustre* was propagated by cloning from samples originally collected in the south of Sweden
128 and *in vitro* cultured (Beike et al., 2015; Di Palma et al., 2016) at the University of Santiago de
129 Compostela (Spain). Propagules of this species were grown in 5 L bioreactors (Applikon
130 Biobundle) under axenic conditions until mature shoots were obtained. Under these
131 conditions, the moss material is grown free of contaminants (see Beike et al., 2015 for more
132 information).
133 Green apical parts of *P. purum* (Ares et al., 2012) and *F. antipyretica* (Debén et al., 2017) were
134 separated by hand for use in the experiments. However, whole shoots of *S. palustre* were
135 used, as all of the plant tissue was green and physiologically active (Beike et al., 2015). The
136 moss material was washed three times with bidistilled water (10 L H_2O for each 100 g dry
137 weight – d.w.) and once with 10 mM EDTA (1 L of solution per 200 g d.w.), always with
138 shaking (20 min, 100 rpm). After blotting on filter paper to remove excess moisture, the
139 moss was devitalized by oven-drying in consecutive cycles (each of 8 h in duration) at 50, 80
140 and 100 ºC (Ares et al., 2012; Debén et al., 2016), as bioconcentration of contaminants mainly
141 involves passive uptake processes that are independent of the vitality of the moss (Giordano
142 et al., 2009; Fernández et al., 2010). The devitalized moss samples were used for physico-
143 chemical characterization of the moss surface and in field experiments, as explained below.
144 *2.2. Physico-chemical characterization of the moss surface*
145 In order to better understand metal accumulation and adsorption processes, the main
146 physico-chemical characteristics of the different moss species, including the chemical
147 composition, nature of the functional groups and surface charge, were determined.
148 2.2.1. Chemical characterization

149 The C, N and H contents in the moss were determined using a LECO TruSpec CHN-1000
150 analyzer. To identify the presence of the different functional groups that characterise the
151 moss surface, ATR-FTIR spectra were collected over the wavenumber range 4000-600 cm^{-1}
152 , with a JASCO FT/IR-4200 spectrophotometer. Samples were ground, mixed
153 homogeneously and placed on a ZnSe ATR crystal plate to facilitate collection of the spectra.
154 For each sample, the spectra were obtained at a resolution of 1 cm^{-1}, from at least 50 co-
155 added scans. For *F. antipyretica*, the spectra were also collected after Cu^{2+} and Cd^{2+} adsorption.
156 2.2.2. Surface acid-base titrations
157 Acid-base titrations of the mosses were conducted at room temperature (~20 ºC) at pH 3-
158 11 under an N_2 atmosphere, following the protocol established by González and Pokrovsky
159 (2014). Briefly, the potentiometric acid-base titrations were performed automatically in two
160 steps (acid and basic regions) with a Crison micropH 2002 pH meter, a Crison microBU
161 2030 burette and a Radiometer GK2401C combination pH electrode, which was calibrated
162 with Crison pH buffers prior to each titration. For the basic titration, 0.2 M NaOH was used
163 as the titrant solution, and for the acid titration, 0.05 M HNO_3 was used. For all titrations, 1
164 g d.w. L^{-1} moss suspensions were prepared in 50 mL of 0.01 M $NaNO_3$. The centrifuged,
165 filtered supernatant collected after conditioning for 1 h was used as the reference solution,
166 and the excess of charge was calculated as the difference between the acid/base
167 concentration in the suspension and in the reference solution (González and Pokrovsky,
168 2014).
169 Acid-base titration curves were obtained by plotting pH against the volume of titrant added
170 to the moss suspension. Surface charge curves were obtained by plotting surface charge (Q
171 in mmol per g of moss) against pH after correction of the blank (mmol of titrant consumed
172 by the supernatant after equilibration of the moss in the electrolyte solution for 1 h). The
173 point of zero charge (PZC) can be read from the surface charge curves at the pH where the
174 net charge on the moss surface equals zero.

As an alternative to the Linear Programming Model (LPM), previously used to determine the proton binding constants of bacteria and natural mosses (Pokrovsky et al., 2008; González and Pokrovsky, 2014), the charging behaviour (Q, surface charge in mmol g^{-1}) was simulated in the present study according to a 2-site Langmuir-Freundlich type model (LF-2pos) (Gondar et al., 2005). While the LPM model considers a large number of proton binding sites, which increases the number of fitting parameters required, the LF-2pos model considers a bimodal distribution (n = 2) of the proton binding affinity to the surface:

$$Q = Q_0 + \sum_{i=1}^{n} \frac{S_i([H^+]K_i)^{m_i}}{1 + ([H^+]K_i)^{m_i}} \quad (1)$$

where Q_0 (mmol g^{-1}) is a parameter needed to account for the position of the surface charge curves on the y-axis, i.e. the initial charge of the surface; S_i is the abundance of the acidic functional groups, in mmol g^{-1}; K_i is the mean value of the proton binding affinity distributions; and m_i defines the heterogeneity of the surface so that a value of 1 leads to a Langmuir type equation. As the distribution is bimodal, the total abundance of acidic functional groups was calculated as the sum of the abundance of the two types of groups: S_1 + S_2 (mmol g^{-1}).

2.2.3. Metal adsorption

Moss suspensions (1 g L^{-1}) were prepared in 0.01M $NaNO_3$ and aliquots of stock metal solutions, i.e. 0.02M $Cu(NO_3)_2$, $Pb(NO_3)_2$ or $Cd(NO_3)$, were added and allowed to equilibrate after buffering with 0.1 M NaOH or HNO_3 to pH 5. The metal concentrations used in the experiments ranged between approximately 1.5×10^{-2} and 1.2 mM for Cu^{2+}, 2×10^{-3} and 0.4 mM for Pb^{2+}, and 4×10^{-3} and 0.4 mM for Cd^{2+}. Previous kinetic experiments established the equilibration time between consecutive additions at 5 – 15 min, depending on the concentration of the metal ion and the type of moss (Di Palma et al., 2016). The pH was measured with a Radiometer GK2401C electrode, which was calibrated using buffer solutions. The free metal concentration in solution after adsorption was measured with ion

199 selective electrodes (ISE) (ELIT Cu 2774; ELIT Cd 3893; ELIT Pb 3886; ELIT 003N LIAC
200 60651) connected to a Crison 2002 pH meter. Routine ISE calibrations were performed
201 using standard solutions of Cu^{2+}, Cd^{2+} and Pb^{2+} over a wide range of metal concentrations,
202 prior to each adsorption experiment, to test the Nernstian response of the electrodes. The
203 concentration of adsorbed metal was determined as the difference between the total amount
204 of metal added initially and the free metal concentration measured in solution. All
205 experiments were replicated (n = 2 or 3) to ensure reproducibility.
206 The results of the metal adsorption experiments were then analysed using empirical models,
207 such as the isotherm equations of Langmuir and Langmuir-Freundlich:

Langmuir model (L): $$q_e = \frac{K_L Q_{max} C_e}{(1 + K_L C_e)} \quad (2)$$

Langmuir-Freundlich model (L-F): $$q_e = \frac{Q_{max}(K_{LF} C_e)^{\frac{1}{n}}}{1 + (K_{LF} C_e)^{\frac{1}{n}}} \quad (3)$$

208 where q_e is the concentration of metal adsorbed on the moss per unit of mass (mg g^{-1}); C_e is
209 the concentration of metal in solution (mg L^{-1}); Q_{max} is the maximum adsorption capacity of
210 the moss species (mg g^{-1}); K_L and K_{LF} are the Langmuir and Langmuir-Freundlich adsorption
211 constants, respectively, which are related to the affinity of the metal for the binding sites on
212 the moss surface; and n is an empirical parameter defining the heterogeneity of the system.
213 Although these adsorption isotherms do not consider ion-exchange as a possible mechanism,
214 they are commonly used in biosorption because interpretable constants can be easily
215 incorporated and provide a broad framework for comparison of different biosorbents
216 (Lodeiro et al., 2004).
217 *2.3. Field experiment*
218 2.3.1. Preparation of moss transplants
219 Devitalized moss samples were used to prepare the transplants. Rectangular flat bags (6 x 4
220 cm) were made from glass fibre mesh (2 mm), previously washed with 30% HNO_3 (24 h) to

221 eliminate any trace contaminants. The moss was placed in the bags (720 mg d.w. and sample
222 density, 15 mg cm^{-2}), which were then sewn with nylon thread, to prevent displacement of
223 the moss inside the bag while minimizing overlapping and compression of the moss (Ares et
224 al., 2012; 2014). The transplants were stored in vacuum-sealed bags until exposure. Three
225 aliquots of moss material from each species were stored for subsequent determination of the
226 initial concentration of the pollutants prior to exposure (t_0) (Couto et al., 2004). Additionally,
227 three transplants of each type (controls) were vacuum sealed and transported to the field to
228 check for contamination during recovery and transportation of the bags at the end of the
229 exposure period.

230 2.3.2. Sampling set-up

231 The study was carried out at eight sampling sites (SS) located in the surroundings of five
232 industrial sites in Galicia (NW Spain) (Fig. 1 and Table SM1, Supporting Material). The sites
233 are characterized as sources of emission of Al, Cd, Cr, Cu, Fe, Hg, Ni, Pb and V to the
234 environment (Varela et al., 2014; García-Seoane et al., 2019). At each SS, three replicates of
235 each type of transplant (i.e. of each moss species, 3 x 3 = 9) were suspended from a fibreglass
236 pole, held perpendicularly over street lamps at 4 m height (following the procedure
237 recommended by Ares et al., 2012). The experiment was carried out between November
238 2016 and January 2017 (exposure period, 8 weeks), i.e. for a long enough period to ensure
239 detection of consistent trace metal uptake in the moss (Capozzi et al., 2016). The exposed
240 transplants were then removed from the poles and immediately stored in plastic bags and
241 transported to the laboratory.

242 2.3.3. Chemical analysis

243 The moss samples were oven dried at 40 ºC, homogenized in an ultracentrifugal mill (Retsch
244 MM400) inside zirconium vessels and stored in glass vials until chemical analysis. Samples
245 were oven-dried again (40 ºC) before analysis and 0.2 g d.w. aliquots were digested with 8
246 mL of HNO_3 (Hiperpur) and 2 mL of H_2O_2 (30%, Sigma Aldrich) in Teflon bombs in a

247 microwave oven (Ethos-1 Milestone). The concentrations of Al, Cd, Co, Cr, Cu, Fe, Ni, Pb
248 and V were determined by inductively coupled plasma mass spectrometry (ICP-MS Agilent
249 7700x). In addition, 0.2 g d.w aliquots of samples were used to determine Hg concentrations
250 in an elemental analyser (Milestone DMA80).
251 Standard reference materials M2 and M3 (terrestrial moss *Pleurozium schreberi*; Steinnes et al.
252 1997) were analysed for quality control of the measurements (once every ten samples). To
253 calculate the percentage error in the analysis, one analytical replicate was also analysed every
254 10 samples. To control for any possible contamination in the analytical process, one blank
255 was included every 10 samples. The analytical quality of data was generally satisfactory.
256 Recovery levels for reference material M2 were 95-105% for Al, Hg and V, 70-95% for Cd,
257 Cr, Ni and Fe, and 55-75% for Co and Pb. For reference material M3, the recovery levels
258 were 95-120% for Al, Fe, Hg and V, 70-95% for Cd and Ni, and 50-70% for Co, Cr, Cu and
259 Pb. The concentrations obtained were always above the limits of quantification (LOQ). The
260 percentage difference between analytical replicates was always less than 10% for each
261 element. The unexposed moss material (t_0 and controls) was analysed following the same
262 procedure as the samples.
263 2.3.4. Data treatment
264 Prior to data analysis, contamination during the transportation process and handling of the
265 bags was checked by comparing the initial concentration of each element in unexposed moss
266 samples (t_0) with control bags using the non-parametric Mann-Whitney U test.
267 Lilliefor's modification of the Kolmogorov-Smirnov and Levene tests were used to check
268 the normality of the data distribution and homogeneity of variances, respectively. As the data
269 were not normally distributed, the non-parametric Scheirer-Ray-Hare test (equivalent to a
270 Two-Way ANOVA; Dytham, 1999) was used to determine whether the concentrations of
271 the different elements varied significantly ($p<0.05$) between sampling sites and moss species.
272 Sampling sites, moss species, as well as their interaction were used as predictors in the

following model: Concentration ~ Sampling site × Species. When significant differences were detected, non-parametric Kruskal-Wallis and Bonferroni post-hoc tests were used to identify homogeneous subgroups. Differences between moss species were further examined in sampling sites classified as "contaminated". Briefly, density distributions were estimated for the concentrations of each element (n = 72) by kernel smoothing. Values on the left side of the modal value (mode) calculated for each distribution were used to generate the values on the right side of a symmetrical distribution. A unimodal distribution was obtained for the subset of data with the lowest concentrations (i.e. unpolluted SS). The 0.99 percentile was subsequently calculated for this new dataset and used as a cut-off value for each element; thus, when elemental concentrations in the samples (for the three moss species) were higher than this value, the SS was categorised as "contaminated". Details of the procedure for selection of contaminated SS can be found in García-Seoane et al. (2019). Statistical analysis was performed in R-3.4.0 statistical software (R Core Team, 2020) using the "FSA" (Ogle et al., 2019), "KernSmooth" (Wand and Ripley, 2006) and "rcompanion" (Mangiafico, 2018) packages. Enrichment of the different contaminants in the transplants was calculated as net enrichment (NE), defined as the difference between the concentrations at the end of the exposure period and the initial concentrations in the moss (t_0) (Couto et al., 2004; Ares et al., 2012).

3. Results

3.1. Chemical characterization

According to the elemental analysis, the *S. palustre* samples contained less C than the *P. purum* and *F. antipyretica* samples (41.2, 44.3 and 44.9%, respectively). No considerable differences in the H content of the mosses were observed (6.44, 6.26 and 6.50%, respectively), although the aquatic species *F. antipyretica* contained almost three times more N (3.70%) than the terrestrial *P. purum* and *S. palustre* (1.14 and 1.31%, respectively).

298 Comparison of the ATR-FTIR spectra of the three mosses (Fig. 2) revealed that most bands
299 are common to all species, which indicates the similarity of the functional groups (see band
300 assignation in Table SM2, Supporting Material). Comparison of the *F. antipyretica* spectra
301 collected before and after adsorption of Cu^{2+} and Cd^{2+} (Fig. SM1, Supporting Material)
302 revealed a slight shift in the wavenumber in some specific bands, which can be attributed to
303 the interaction between functional groups on the surface of the mosses and the heavy metals
304 (Table 1). The bands generated by the vibration of single bonds involving O atoms (alcohols
305 or carboxylic groups) were equally shifted after Cu and Cd adsorption, indicating that these
306 functional groups participate in the adsorption of both metals. On the other hand, bands due
307 to aliphatic C–H vibrations are not affected by the adsorption process, indicating that these
308 groups do not participate in the process.

309 *3.2. Surface charge behaviour*

310 The acid-base titration curves and the corresponding PZC values for the different moss
311 species are shown in Fig. 3. The PZC values obtained for the studied species ranged in a
312 narrow pH interval (0.24 pH units): *F. antipyretica* (4.51); *P. purum* (4.60) and *S. palustre* (4.75).
313 Among the different moss species, *S. palustre* showed a greater change in the surface charge
314 in the pH range studied, while *F. antipyretica* showed the lowest change in the surface charge.
315 The change in the surface charge was calculated as the sum, in absolute values, of the highest
316 and the lowest values of the charge for each moss in the surface charge curve at pH 3–10.
317 The following approximate values were obtained (mmol g^{-1}): *S. palustre* (~0.74) > *P. purum*
318 (~0.62) > *F. antipyretica* (~0.36).

319 As indicated above, the surface charge curves (Fig. 3) were simulated using the 2-site
320 Langmuir-Freundlich equation (equation 1). From the fitting results (Table 2), the total
321 abundance of acidic functional groups in the mosses differed in the following decreasing
322 order: *S. palustre* (1.93) > *P. purum* (1.68) > *F. antipyretica* (0.41). The $log\ K_1$ values ranged
323 between 2.67 and 3.97, and the $log\ K_2$ values ranged between 7.86 and 11.08, with *S. palustre*

showing the highest values for both constants. The abundance of functional groups was also calculated by the LPM model, which included 8 to 9 functional groups and 17 to 19 fitting parameters (whereas the simplified LF-2pos model only included 2 functional groups and 7 fitting parameters). The total abundance of functional groups calculated using both models was different, normally higher with the LF-2pos model, but there was a good linear correlation between the models (r^2 = 0.9998, p<0.01). In addition, the total concentration of acidic binding sites (S_1 + S_2, equation 1) was directly related to the PZC in the mosses.

3.3. Metal adsorption isotherms

The adsorption experiments conducted in aqueous media showed the same trend in the retention capacity of Cu, Cd and Pb at pH 5 in all mosses for (Fig. 4): *S. palustre* > *P. purum* > *F. antipyretica*. As observed from the surface charge of the mosses, *S. palustre* exhibited the highest absolute and negative surface charge, which makes it the most efficient adsorbent for metal cations, since it has the highest density of negatively charged sites on the surface. By contrast, *F. antipyretica*, which has the lowest absolute and negative surface charge, should be the poorest metal cation adsorbent. As observed in Table 3, comparison of the maximum adsorption capacity (Q_{max}) of a given moss for the three metals shows that the general trend followed the order Pb > Cu > Cd (Table 3 and Fig. SM2, Supporting Material), although in *S. palustre* the highest Q_{max} corresponded to Cu. Finally, the aquatic moss (*F. antipyretica*) showed a lower capacity than the terrestrial mosses to adsorb the selected trace metals.

Another significant relationship between the abundance of proton binding sites on the mosses surface and the corresponding adsorption capacity to remove metals from aqueous systems can be established (Fig. SM3, Supporting Material). This effect appeared to be more pronounced for Cu (y = 12.859x + 17.023; r^2 = 0.885, p<0.1), with a slope which is approximately 5 times the Cd slope (y = 2.724x + 6.110; r^2 = 0.894, p<0.1) and 2 times the Pb slope (y = 7.781x + 28.014; r^2 = 0.948, p<0.05).

3.4. Field experiment

350 The Mann-Whitney U test did not indicate any significant differences (p<0.05) between t_0
351 (see initial concentrations in the moss in Table SM3, Supporting Material) and control bags,
352 and there was therefore no evidence of sample contamination during transportation and
353 handling (Table SM4, Supporting Material).
354 The results (Fig.1) showed net enrichment of the different elements determined in the three
355 moss species at each sampling site. At the end of the exposure period, metal enrichment was
356 observed at all sites, except for Co in *F. antipyretica* (in SS2-SS8) and Ni in the same species
357 (in SS7 and SS8). The Scheirer-Ray-Hare test showed that there was no significant first-order
358 Sampling site × Species interaction (p>0.05) (Table SM5, Supporting Material). However,
359 significant differences were detected between SS for all the elements measured (p<0.05;
360 Table SM5, Supporting Material). Significant differences between the three moss species
361 (p<0.05) were also found for net enrichment of Cd, Co, Hg and Ni (Fig. 1; Table SM5,
362 Supporting Material). No significant differences between species were found for the other
363 elements. A more detailed evaluation of the net enrichment (Fig. 1) revealed that, although
364 not always significant, the elements displayed the same inter-species differences in most of
365 the sampling sites: i) *S. palustre* > *P. purum* > *F. antipyretica* (Al, Cd, Co, Fe and Ni); ii) *S. palustre*
366 > *P. purum* = *F. antipyretica* (Cr, Cu and Pb); and iii) *F. antipyretica* >>> *P. purum* = *S. palustre*
367 (Hg). No clear differences between species were observed for V. The 0.99 percentile values
368 calculated for each element are also shown (Fig. 1). In all three moss species, net enrichment
369 exceeded the percentile value calculated for Al (in SS1 and SS4), Cd (SS1 and SS6), Co (SS1),
370 Cr (SS5 and SS6), Pb (SS1, SS5 and SS6) and V (SS4), thus distinguishing these SS as the
371 most polluted by these elements. Except for Pb in SS1 and V in SS4, net enrichment in these
372 polluted sites was highest in *S. palustre*.

373 **4. Discussion**

374 Regarding the practical objective of using *F. antipyretica* to monitor air pollution, the clear
375 conclusion reached from the results of both the laboratory and field experiments is that,

376 except for monitoring Hg (for which using this species is recommended), we encourage to
377 use preferably one of the two terrestrial mosses. The ranking of the species regarding the
378 concentrations reached was generally the same (i.e. *S. palustre* > *P. purum* > *F. antipyretica*),
379 both in laboratory experiments (adsorption of Cd, Cu and Pb conducted in aqueous medium)
380 and in the field experiments, for most of the elements (significantly for Cd, Co and Ni in *S.*
381 *palustre* > *F. antipyretica*), except Hg (discussed later). However, although the previous
382 sequence was altered in the surroundings of certain industries, the order was maintained for
383 elements such as Al, Cu and Fe regardless of the level of pollution detected. In addition, Cr
384 and Pb concentrations were higher in *S. palustre* than in the other species, while for V the
385 results are not clear.
386 A possible explanation for these results is that the species are ranked in the same way in
387 relation to i) PZC (Fig. 3), ii) change in the surface charge in the pH range studied (Fig. 3),
388 iii) abundance of functional groups with acidic character (Table 2) and iv) the values obtained
389 for $log\ K_1$ and for $log\ K_2$ (with the exception of $log\ K_1$, the value of which was higher in *F.*
390 *antipyretica* than in *P. purum*). The results of the acid-base titrations are similar to those
391 obtained by González and Pokrovsky (2014) and González et al. (2016). The PZC and the
392 abundance of proton binding sites obtained by these authors for *P. purum* were 4.96 and 0.55
393 mmol g^{-1}, respectively. Whereas González and Pokrovsky (2014) and González et al. (2016)
394 used a non-linear fit (LPM), the present study used a simplified model (LF-2pos), supported
395 by the information extracted from the ATR-FTIR spectra. This technique suggests that
396 oxygenated groups including carboxylic and alcoholic or phenolic functional groups are the
397 main groups participating in metal binding. Previous studies confirmed that these groups
398 participated in Cu binding in *Sphagnum* peat mosses (Gardea-Torresdey et al., 1996; Tipping
399 et al., 2008; González and Pokrovsky, 2014). Brown (1982) attributed an array of surface
400 binding sites in bryophytes similar to that used for humic substances, i.e. carboxylic acid
401 groups and weaker oxygen-based ligands such as phenolic ligands. Considering these

similarities, use of humic acids as surrogates to describe bryophyte binding sites is valid (Tipping et al., 2008) and application of a model previously used for humic and fulvic acids, i.e. the LF-2pos equation (Gondar et al., 2005), seems appropriate for explaining the acid-base reactions in moss tissues. The advantage of this model over the LPM is that it can be used even when the number of data points in the acid-base titration of the moss tissue is limited. The good linear correlation between both models indicates that the comparison is feasible. The aquatic moss *F. antipyretica* falls in the lower range of the total concentration of acidic binding sites ($S_1 + S_2$, equation 1) and the PZC. Although the PZC was similar in all the mosses, the aquatic and terrestrial mosses differ in regard to the abundance of proton binding sites, with the terrestrial species shifting towards higher values. The first protonation constant was similar in the aquatic and terrestrial mosses, but *F. antipyretica* showed a much lower log K_2 value (7.86) than the terrestrial species (approximately 11). This difference may also be related to the different metal binding behaviour observed for this aquatic species.

Although the Langmuir and Langmuir-Freundlich isotherm models were equally valid for describing metal binding on the mosses, according to the correlation coefficient and RMSE values (Table 3 and Table SM6, Supporting Material), the logarithmic plot of the adsorbed against solution concentrations provided a better fit at low metal loadings when the Langmuir-Freundlich equation is used (Fig. SM4, Supporting Material). This indicates that the moss surface shows intermediate behaviour between purely Langmuir and purely Freundlich models (Koopal et al., 2020). The metal binding capacity varies according to the moss species and the targeted trace metal. Thus, the maximum adsorption capacity (mg g^{-1}) ranged from 23.1-45.2, 31.0-42.7 and 7.39-12.1, for Cu, Pb and Cd respectively. These values are similar to those determined in other studies with terrestrial and aquatic mosses (Vázquez et al., 1999; Martins et al., 2004; Sari et al., 2008; González et al., 2016; Di Palma et al., 2019). González and Pokrovsky (2014) reported a similar trend regarding the relative binding capacity of mosses for these metals. In general, Cd showed lower affinity for the moss

surface, while Cu and Pb showed similar affinities. Among the studied mosses, *F. antipyretica* showed lower metal binding capacity, which is consistent with the surface charge behaviour of this moss species, i.e. lower total surface charge and lower abundance of proton binding sites. In biomonitoring studies using mosses, the strongest relationships between atmospheric deposition and moss metals content were obtained for Cd and Pb (Aboal et al., 2010), which probably explains why these metals are included in many studies. In the case of *S. palustre*, which belongs to the genus most commonly used in biomonitoring, these two elements show the highest affinities based on the values of the $log\ K_{LF}$ (Table 3); this also happens for *F. antipyretica* and similarly for *P. purum* (although in this case the affinity constant of Cu is similar to that of Cd). However, the results obtained for the maximum adsorption capacity (Q_{max}) cannot be explained in this way because for all moss species the binding capacity was higher for Cu than for Cd.

Exceptionally, for Hg, the order of the concentrations reached in the field seems to be the opposite of the aforementioned trend (i.e. *F. antipyretica* > *P. purum* > *S. palustre*), as previously observed in comparisons of species of the genus *Sphagnum* with *P. purum* (Ares et al., 2014; Capozzi et al., 2017). This element differs from the other metals studied given its electronic characteristics, such as its ionic radius and especially its very high covalent index, which makes it a Class B element (nitrogen/sulphur-seeking metal ions; for further detail see Nieboer and Richardson, 1980). Unlike the other elements (mostly borderline, intermediate preference, except for Al, which is a Class A, oxygen-seeking metal ion) in which the adsorption process seems to be almost exclusively due to the carboxylic and alcoholic or phenolic groups, adsorption of Hg is due to other groups. Pérez-Llamazares et al. (2009) verified the very strong affinity of the -SH group for this element in *P. purum*, although it could also be due to amine (the N concentration is three times higher in *F. antipyretica* than in the other two species) and polyphenol binding sites. Unfortunately, no differences were

found between the moss species in the ATR-FTIR spectra at the wavelengths corresponding to these groups.

The tendency of *Sphagnum* species to display a higher uptake capacity than *P. purum* under field conditions has already been reported. Ares et al. (2014) observed this by comparing the uptake capacity of *S. denticulatum* and *P. purum* for Cd, Cu and Pb, obtaining less clear results for Zn. Capozzi et al. (2017) also showed this trend with the same species used in the present study, concluding that *S. palustre* has a greater loading capacity for Al, Ba, Cu, Hg, Pb and Sr. However, this is a generalization, and biomonitoring results always reveal exceptions in different industrial environments. The reason for the difference between the results of the laboratory and some of the field experiments -in relation to the order in which the species are ranked- is that in the latter case, in addition to the adsorption processes, the amount of particulate material that these species are able to retain on their surfaces also plays a role. In this experiment the mosses were devitalised, so that differences in metabolic contribution or intracellular transport can be disregarded.

On the other hand, it is important to consider that field experiments involve a multicomponent system in which the different metal cations are competing for the same binding sites on the moss surface, whereas only single-cation adsorption systems have been monitored in laboratory experiments. Thus, there is clearly an interaction between the characteristics of the pollutants (e.g. dissolved metals, particulate matter, and the fingerprint of the metal concentration that would affect competition) and the moss species. This would explain why Debén et al. (2017) obtained higher metal concentrations in *F. antipyretica* than in *S. denticulatum* in aquatic environments, despite the lower adsorption capacity of the former species in the laboratory, as it has recently been proven that particulate material largely contributes to metal concentrations in *F. antipyretica*, sometimes more than 40% of the total in the moss (Real et al., 2021). From a methodological point of view, distinguishing the contribution made by particles and adsorbed material to moss metal loads is still far from

being resolved (Pérez-Llamazares et al., 2013; Spagnuolo et al., 2013) and appears complex, since the capacity to retain particles may be related to the specific surface area which, in turn, may depend on the number of binding sites. Thus, it is difficult to differentiate the metal load due to particle retention from that due to adsorption, as species with a larger specific surface area (e.g. *S. palustre*) will have more binding sites.

5. Conclusions

The moss species studied differ in their affinity for the elements considered (i.e. related to atomic properties and the solution chemistry of metal ions, grouping metal ions according to their binding preferences). In the atmospheric environment, *S. palustre* (but also *P. purum*) seem to be the best choices for biomonitoring Class A elements (oxygen-seeking metal ions) or borderline elements (intermediate preference for O- and N- or S- ligands), while *F. antipyretica* is the most suitable for biomonitoring Hg (classified as Class B, nitrogen/sulphur-seeking metal ion). This is due to differences in physico-chemical characteristics, especially the density of ligands, with much greater numbers of oxygenated groups involving carboxylic and alcoholic or phenolic functional groups in *S. palustre*, followed by *P. purum.* Thiol, amine and polyphenol groups are probably more abundant in *F. antipyretica*, although further research is required to clarify this.

The results of the laboratory experiments (acid-base titrations and metal adsorption experiments) highlighted the relationship between metal concentrations and moss characteristics: i) point of zero charge; ii) change in the surface charge in the pH range studied; iii) abundance of functional groups with acidic character; and iv) the values obtained for $log\ K_1$ and for $log\ K_2$. Furthermore, the LF-2pos equation (model previously used for humic and fulvic acids) provided optimal results for simulating proton binding in mosses.

The concentrations reached in the exposed mosses indicate that metal uptake processes not only depend on the physico-chemical characteristics of the mosses, but are also influenced by the specific characteristics of the industrial scenario and maybe also by the environment

of origin of the mosses, i.e. terrestrial or aquatic. The underlying causes may include competition between different metal cations for the moss surface binding sites, the nature of the metal cations (particulate or dissolved) or both. In addition, the relationship between the amount of metal retained by the mosses and the abundance of surface sites confirms that proton/metal competition is a major driver of metal bioconcentration in bryophytes. Laboratory experiments should be extended to a wider range of metals in order to assess the usefulness of this correlation as a tool for predicting the metal uptake capacity of different mosses.

Acknowledgments

R. García-Seoane was supported by a postdoctoral research grant awarded by the Juan de la Cierva-Formación (FJC2019-040921-I), funded by MCIN/AEI/10.13039/501100011033 (Spain) and EU NextGenerationEU/PRTR programmes. S. Fiol and J. Antelo acknowledge financial support provided by the Xunta de Galicia - Consellería de Educación e Ordenación Universitaria (Consolidation of Competitive Research Groups; GI-1245, ED431C 2022/40). J.R. Aboal and J.A. Fernández acknowledge financial support provided by the Xunta de Galicia - Consellería de Educación e Ordenación Universitaria (Consolidation of Competitive Research Groups; GI-1252, ED431C 2020/19). The manuscript benefitted substantially from the critical comments of two anonymous reviewers.

Author contributions

Conceptualization: S. Fiol, J.R. Aboal; Formal Analysis: S. Fiol, J. Antelo, R. García-Seoane; Investigation: S. Fiol, J. Antelo, R. García-Seoane; Methodology: S. Fiol, J. Antelo, J.A. Fernández, J.R. Aboal; Resources: S. Fiol, J.A. Fernández, J.R. Aboal; Writing - original draft: S. Fiol, R. García-Seoane, J.R. Aboal; Writing – review & editing: J. Antelo, J.A. Fernández. All authors reviewed and approved the final version of the manuscript.

Competing Interest Declaration

The authors declare that they have no competing financial or non-financial interests that could have influence the work reported in this paper.

6. References

Aboal, J.R., Fernández, J.A., Boquete, T., Carballeira, A., 2010. Is it possible to estimate atmospheric deposition of heavy metals by analysis of terrestrial mosses? Sci. Total Environ. 408(24), 6291-6297. https://doi.org/10.1016/j.scitotenv.2010.09.013

Adamo, P., Crisafulli, P., Giordano, S., Minganti, V., Modenesi, P., Monaci, F., 2007. Lichen and moss bags as monitoring devices in urban areas. Part II: trace element content in living and dead biomonitors and comparison with synthetic materials. Environ. Pollut. 146(2), 392-399. https://doi.org/10.1016/j.envpol.2006.03.047

Ares, A., Aboal, J.R., Carballeira, A., Giordano, S., Adamo, P., Fernández, J.A., 2012. Moss bag biomonitoring: a methodological review. Sci. Total Environ. 432, 143-158. https://doi.org/10.1016/j.scitotenv.2012.05.087

Ares, A., Fernández, J.A., Carballeira, A., Aboal, J. R., 2014. Towards the methodological optimization of the moss bag technique in terms of contaminants concentrations and replicability values. Atmos. Environ. 94, 496-507. https://doi.org/10.1016/j.atmosenv.2014.05.066

Beike, A.K., Spagnuolo, V., Lüth, V., Steinhart, F., Ramos-Gomez, J., Krebs, M., Adamo, P., Rey-Asensio, A.I., Fernández, J.A., Giordano, S., Decker, E.L., Reski, R., 2015. Clonal in vitro propagation of peat mosses (*Sphagnum* L.) as novel green resources for basic and applied research. Plant Cell Tissue Organ Cult. 120(3), 1037-1049. https://doi.org/10.1007/s11240-014-0658-2

Brown, D.H., 1982. Mineral nutrition. In: Smith, A.J.E. (Ed.) Bryophyte Ecology. Chapman & Hall, London.

554 Capozzi, F., Giordano, S., Aboal, J.R., Adamo, P., Bargagli, R., Boquete, T., Di Palma, A.,
555 Real, C., Reski, R., Spagnuolo, V., Tretiach, M., Varela, Z., Zechmeister, H.,
556 Fernández, J.A., Steinbauer, K., 2016. Best options for the exposure of traditional and
557 innovative moss bags: A systematic evaluation in three European countries. Environ.
558 Pollut. 214, 362-373. https://doi.org/10.1016/j.envpol.2016.04.043
559 Capozzi, F., Adamo, P., Di Palma, A., Aboal, J.R., Bargagli, R., Fernández, J.A., Lopez Mahia,
560 P, Tretiach, M., Spagnuolo, V., Giordano, S., 2017. *Sphagnum palustre* clone vs native
561 *Pseudoscleropodium purum*: A first trial in the field to validate the future of the moss bag
562 technique. Environ. Pollut. 225, 323-328.
563 https://doi.org/10.1016/j.envpol.2017.02.057
564 Carvajal, B., Aboal, J.R., Fernández, J.A., Real, C., Carballeira, A., 2010. Influence of roads
565 and inhabited areas on metal concentrations in terrestrial mosses. Atmos. Environ. 44,
566 3432-3441. https://doi.org/10.1016/j.atmosenv.2010.06.007
567 Comess, S., Donovan, G., Gatziolis, D., Deziel, N.C., 2021. Exposure to atmospheric metals
568 using moss bioindicators and neonatal health outcomes in Portland, Oregon. Environ.
569 Pollut. 284. https://doi.org/10.1016/j.envpol.2021.117343
570 Couto, J.A., Aboal, J.R., Fernandez, J.A., Carballeira, A., 2004. A new method for testing the
571 sensitivity of active biomonitoring: an example of its application to a terrestrial moss.
572 Chemosphere 57, 303-308. https://doi.org/10.1016/j.chemosphere.2004.05.036
573 Davis, T.A., Volesky, B., Mucci, A., 2003. A review of the biochemistry of heavy metal
574 biosorption by brown algae. Water Res. 37, 4311-4330.
575 https://doi.org/10.1016/S0043-1354(03)00293-8
576 Debén, S., Fernández, J.A., Carballeira, A., Aboal, J.R., 2016. Using devitalized moss for
577 active biomonitoring of water pollution. Environ. Pollut. 210, 315-322.
578 https://doi.org/10.1016/j.envpol.2016.01.009

579 Debén, S., Aboal, J.R., Carballeira, A., Cesa, M., Fernández, J.A., 2017. Monitoring river
580 water quality with transplanted bryophytes: A methodological review. Ecol. Indic. 81,
581 461-470. https://doi.org/10.1016/j.ecolind.2017.06.014
582 Di Palma, A., Crespo Pardo, D., Spagnuolo, V., Adamo, P., Bargagli, R., Cafasso, D.,
583 Capozzi, F., Aboal, J.R., González, A.G., Pokrovsky, O., Beike, A.K., Reski, R.,
584 Tretiach, M., Varela., Z., Giordano, S., 2016. Molecular and chemical characterization
585 of a *Sphagnum palustre* clone: Key steps towards a standardized and sustainable moss
586 bag technique. Ecol. Ind. 71, 388-397. https://doi.org/10.1016/j.ecolind.2016.06.044
587 Di Palma, A., González, A.G., Adamo, P., Giordano, S., Reski, R., Pokrovsky, O., 2019.
588 Biosurface properties and lead adsorption in a clone of *Sphagnum palustre* (Mosses):
589 Towards a unified protocol of biomonitoring of airborne heavy metal pollution.
590 Chemosphere 236, 124357. https://doi.org/10.1016/j.chemosphere.2019.124375
591 Donovan, G.H., Jovan, S.E., Gatziolis, D., Burstyn, I., Michael, Y.L., Monleon, V.J., 2016.
592 Using an epiphytic moss to identify previously unknown sources of atmospheric
593 cadmium pollution. Sci. Total Environ. 559, 84-93.
594 https://doi.org/10.1016/j.scitotenv.2016.03.182
595 Dytham, C., 1999. Choosing and Using Statistics: a Biologist's Guide. Blackwell Science Ltd,
596 Oxford, UK.
597 European Pollutant Release and Transfer Register (E-PRTR, 2019). URL
598 http://www.prtres.es/. Accessed 20 June 2021.
599 Fernández, J.A., Ares, A., Rey-Asensio, A. Carballeira, A., Aboal, J.R., 2009. Effect of growth
600 on active biomonitoring with terrestrial mosses. J. Atmos. Chem. 63, 1–11.
601 https://doi.org/10.1007/s10874-010-9152-3
602 García-Seoane, R., Fernández, J.A., Chilà, A., Aboal, J.R., 2019. Improving the uptake of
603 pollutants in moss bags: The wind effect. Ecol. Indic. 107, 105577.
604 https://doi.org/10.1016/j.ecolind.2019.105577

605 Gardea-Torresdey, J.L., Tang, L., Salvador, J.M., 1996. Copper adsorption by esterified and
606 unesterified fractions of *Sphagnum* peat moss and its different humic substances. J. Haz.
607 Mat. 48, 191-206. https://doi.org/10.1016/0304-3894(95)00156-5
608 Giordano, S., Adamo, P., Monaci, F., Pittao, E., Tretiach, M., Bargagli, R., 2009. Bags with
609 oven-dried moss for the active monitoring of airborne trace elements in urban areas.
610 Environ. Pollut. 157, 2798-2805. https://doi.org/10.1016/j.envpol.2009.04.020
611 Gondar, D., López, R., Fiol, S., Antelo, J.M., Arce, F., 2005. Characterization and acid-base
612 properties of fulvic and humic acids isolated from two horizons of an ombrotrophic
613 peat bog. Geoderma 126, 367-374. https://doi.org/10.1016/j.geoderma.2004.10.006
614 González, A.G., Pokrovsky, O.S. (2014). Metal adsorption on mosses: toward a universal
615 adsorption model. J. Colloid Interface Sci., 415, 169-178.
616 http://dx.doi.org/10.1016/j.jcis.2013.10.028
617 González, A.G., Pokrovsky, O.S., Beike, K.A., Reski, R., Di Palma, A., Adamo, P., Giordano,
618 S., Fernández, J.A., 2016. Metal and proton adsorption capacities of natural and cloned
619 *Sphagnum* mosses. J. Colloid Interface Sci., 461, 326-334.
620 http://dx.doi.org/10.1016/j.jcis.2015.09.012
621 He, J., Paul Chen J., 2014. A comprehensive review on biosorption of heavy metals by algal
622 biomass: Materials, performances, chemistry, and modeling simulation tools.
623 Bioresour. Technol. 160, 67-78. https://doi.org/10.1016/j.biortech.2014.01.068
624 Ho, Y.S., McKay, G., 2000. The kinetics of sorption of divalent metal ions onto *Sphagnum*
625 moss peat. Water Res., 34, 735-742. https://doi.org/10.1016/S0043-1354(99)00232-8
626 Koopal, L., Tan, W., Avena, M., 2020. Equilibrium mono- and multicomponent adsorption
627 models: From homogeneous ideal to heterogeneous non-ideal binding. Adv. Colloid
628 Interfac. 280, 102-138. https://doi.org/10.1016/j.cis.2020.102138
629 Lodeiro, P., Cordero, B., Grille, Z., Herrero, R., Sastre de Vicente, M.E., 2004.
630 Physicochemical studies of cadmium(II) biosorption by the invasive alga in Europe,

631 *Sargassum muticum*. Biotechnol. Bioeng. 88, 237-247.
632 https://doi.org/10.1002/bit.20229
633 Mangiafico, S., 2018. rcompanion: Functions to Support Extension Education Program
634 Evaluation. R package version 1(13), 2.
635 Martins, R.J.E., Pardo, R., Boaventura, R.A.R., 2004. Cadmium(II) and zinc(II) adsorption
636 by the aquatic moss *Fontinalis antipyretica*: effect of temperature, pH and water hardness.
637 Water Res. 38, 693-699. https://doi.org/10.1016/j.watres.2003.10.013
638 Nieboer, E., Richardson, D.H., 1980. The replacement of the nondescript term 'heavy
639 metals' by a biologically and chemically significant classification of metal ions. Environ.
640 Pollut. B Chem. Phys. 1, 3-26. https://doi.org/10.1016/0143-148X(80)90017-8
641 Ogle, D.H., Wheeler, P., Dinno, A., 2019. FSA: Fisheries Stock Analysis. R package version
642 (8), 23.
643 Pérez-Llamazares, A., Fernández, J.A., Aboal, J.R., Carballeira, A., 2009. A search for an
644 extracellular extractant of Hg for use in the sequential elution technique with
645 *Pseudoscleropodium purum*. J. Bryol. 31(1), 23-29.
646 https://doi.org/10.1179/174328209X404899
647 Pérez-Llamazares, A., Fernández, J.A., Aboal, J.R., Giordano, S., Carballeira, A., 2013.
648 Evaluation of the efficacy of the sequential elution technique, by use of electron
649 microscopy methods. J. Bryol. 33(1), 54-61.
650 https://doi.org/10.1179/037366810X12814321877543
651 Pokrovsky, O.S., Martinez, R.E., Golubev, S.V., Kompantseva, E.I., Shirokova, L.S., 2008.
652 Adsorption of metals and protons on *Gloeocapsa* sp. cyanobacteria: A surface speciation
653 approach. Appl. Geochem. 23, 2574-2588.
654 https://doi.org/10.1016/j.apgeochem.2008.05.007
655 Priyadarshanee, M., Das, S., 2021. Biosorption and removal of toxic heavy metals by metal
656 tolerating bacteria for bioremediation of metal contamination: A comprehensive

review. J. Environ. Chem. Eng. 9, 104686. https://doi.org/10.1016/j.jece.2020.104686

R Core Team, 2020. R: A language and environment for statistical computing. R Foundation for Statistical Computing, Vienna, Austria. https://www.R-project.org

Real, C., Vázquez, M.D., Villares, R., 2021. An efficient method to wash out the particulate matter trapped by aquatic mosses. Ecol. Indic. 131, 108192. https://doi.org/10.1016/j.ecolind.2021.108192

Sari, A., Mendil, D., Tuzen, M., Soylak, M., 2008. Biosorption of Cd(II) and Cr(III) from aqueous solution by moss (*Hylocomium splendens*) biomass: Equilibrium, kinetic and thermodynamic studies. Chem. Eng. J. 144, 1-9. https://doi.org/10.1016/j.cej.2007.12.020

Shahid, M., Dumat, C., Khalid, S., Schreck, E., Xiong, T., Niazi, N.K., 2017. Foliar heavy metal uptake, toxicity and detoxification in plants: A comparison of foliar and root metal uptake. J. Haz. Mat. 325, 36-58. https://doi.org/10.1016/j.jhazmat.2016.11.063

Spagnuolo, V., Giordano, S., Pérez-Llamazares, A., Ares, A., Carballeira, A., Fernández, J.A., Aboal, J.R., 2013. Distinguishing metal bioconcentration from particulate matter in moss tissue: testing methods of removing particles attached to the moss surface. Sci. Total Environ. 463-464, 727-733. https://doi.org/10.1016/j.scitotenv.2013.05.061

Steinnes, E., Rühling, A., Lippo, H., Mäkinen, A., 1997. Reference materials for large-scale metal deposition surveys. Accred. Qual. Assur. 2, 243-249. https://doi.org/10.1007/s007690050141

Tipping, E., Vincent, C.D., Lawlor, A.J., Lofts, S., 2008. Metal accumulation by stream bryophytes, related to chemical speciation. Environ. Pollut. 156, 936-943. https://doi.org/10.1016/j.envpol.2008.05.010

Varela, Z., Aboal, J.R., Carballeira, A., Real, C., Fernández, J.A., 2014. Use of a moss biomonitoring method to compile emission inventories for small-scale industries. J. Hazard. Mater. 275, 72-78. https://doi.org/10.1016/j.jhazmat.2014.04.061

Varela, Z., Boquete, M.T., Fernández, J.A., Martínez-Abaigar, J., Núñez-Olivera E., Aboal, J.R. 2023. Mythbusters: unravelling the pollutant uptake processes in mosses for air quality biomonitoring. Ecol. Indic. 148, 110095. https://doi.org/10.1016/j.ecolind.2023.110095

Vázquez, M.D., López, J., Carballeira, A., 1999. Uptake of heavy metals to the extracellular and intracellular compartments in three species of aquatic bryophyte. Ecotoxicol. Environ. Saf. 44, 12-24. https://doi.org/10.1006/eesa.1999.1798

Wand, M., Ripley, B., 2006. KernSmooth: Functions for kernel smoothing for Wand & Jones (1995). R package version 2, 22-119.

Xue, Y., Wang, L., Zhang, Y., Zhao, Y., Liu, Y., 2022. Air pollution: A culprit of lung cancer. J. Hazard. Mater. 434, 128937. https://doi.org/10.1016/j.jhazmat.2022.128937

707

708

709 **Tables**

710 **Table 1.** Comparison of some characteristic wavenumbers of the *Fontinalis antipyretica* ATR–
711 FTIR spectra before and after Cu^{2+} or Cd^{2+} adsorption. Shift–Me indicates the shift in
712 wavenumber before and after Cu^{2+} or Cd^{2+} adsorption; Δ(Cu–Cd) shift represents the
713 difference between the shifts in the wavenumbers observed after Cu and Cd adsorption.

714

Wavenumber (cm^{-1})						Assignation
Before adsorption	**After Cu adsorption**	**After Cd adsorption**	**Shift–Cu**	**Shift–Cd**	**Δ(Cu–Cd) shift**	
3344	3334	3334	10	10	0	O-H, N-H
2922	2920	2924	2	− 2	− 4	C-H in CH_3 and CH_2
1543	1542	1539	1	4	3	C=O
1372	1372	1373	0	− 1	− 1	Aliphatic C-H
1239	1243	1243	− 4	− 4	0	C-C and C-O
1028	1025	1025	3	3	0	O-H, C-O in secondary alcohols and ethers

715

716 **Table 2**. Acid-base fitting parameters of the 2-position Langmuir-Freundlich model for

717 *Sphagnum palustre, Pseudoscleropodium purum* and *Fontinalis antipyretica*. d.w.: dry weight.

718

	S. palustre	***P. purum***	***F. antipyretica***
$log\ K_1$	3.97	2.67	3.72
$log\ K_2$	11.08	10.98	7.86
S_1 (mmol g^{-1} d.w.)	1.04	0.75	0.16
S_2 (mmol g^{-1} d.w.)	0.89	0.93	0.25
m_1	0.28	0.57	0.95
m_2	0.98	0.23	0.48
R^2	0.998	0.999	0.998
RMSE	0.019	0.002	8x10-4

719

720 **Table 3**. Langmuir-Freundlich fitting parameters for the adsorption of Cu, Cd and Pb by

721 *Sphagnum palustre, Pseudoscleropodium purum* and *Fontinalis antipyretica*.

722

		S. palustre	***P. purum***	***F. antipyretica***
Cu	$log\ K_{LF}$	0.12	0.20	0.05
	Q_{max} (mg g^{-1})	45.2	34.6	23.1
	n	1.64	1.55	2.58
	R^2	0.99	0.98	0.98
	RMSE	26.9	48.02	21.1
Cd	$log\ K_{LF}$	0.31	0.18	0.19
	Q_{max} (mg g^{-1})	12.1	9.87	7.39
	n	1.04	1.02	1.10
	R^2	0.99	0.99	0.99
	RMSE	2.178	2.659	0.641
Pb	$log\ K_{LF}$	0.28	0.29	0.23
	Q_{max} (mg g^{-1})	40.7	42.7	31.0
	n	1.11	0.80	0.94
	R^2	0.98	0.99	0.97
	RMSE	102.2	34.5	113.2

723

724 **Figure captions**

725 **Fig. 1.** Net enrichment ± SE (n=3) of Al, Cd, Co, Cr, Cu, Fe, Hg, Ni, Pb and V found in
726 moss transplants of the species *Sphagnum palustre* (*Sp*, light grey bars), *Pseudoscleropodium purum*
727 (*Pp*, black bars) and *Fontinalis antipyretica* (*Fa*, white bars) exposed in the sampling sites (1-8)
728 under study. Enrichment of Al and Fe is expressed in mg g^{-1} dry weight (d.w.), while
729 enrichment of Cd, Co, Cr, Cu, Hg, Ni, Pb and V is expressed in μg g^{-1} d.w. Horizontal
730 dashed lines correspond to the 0.99 percentile value calculated for each element (see section
731 2.3.4.). Vertical dashed lines group the SS by their proximity to the 5 industries under study
732 (further details in Table SM1). Asterisks indicate significant differences between species
733 according to the Bonferroni post-hoc test (*: p<0.05). Note: vertical axes have been cut off
734 in Cd, Co, Cr, Fe, Pb and V plots to facilitate interpretation of the data. At the bottom of
735 this figure, map showing the location of the study area in NW Spain and the eight selected
736 sampling sites affected by different degrees of industrial contamination (A): FS, ferrous-
737 smelter; CF, ceramic factory; PW, paper and wood production with cogeneration; and PP,
738 coal-fired power plant. (i) and (ii) refer to two different industries with the same activity (to
739 facilitate interpretation of the colours used in this figure legend, see the online version of this
740 article).

741 **Fig. 2**. ATR-FTIR spectra of the three native mosses *Sphagnum palustre, Pseudoscleropodium*
742 *purum* and *Fontinalis antipyretica* in the region 1800 – 900 cm^{-1} showing the main peaks
743 assignation.

744 **Fig. 3**. Surface charge vs. pH curves derived from the acid-base titration of the moss species
745 *Sphagnum palustre, Pseudoscleropodium purum* and *Fontinalis antipyretica* in 0.01 M $NaNO_3$ using 1
746 g dry weight L^{-1} biomass. The lines represent the fits of the 2-site Langmuir-Freundlich model
747 (see text for further details).

748 **Fig. 4**. Metal adsorption on the moss species *Sphagnum palustre, Pseudoscleropodium purum* and
749 *Fontinalis antipyretica* at pH 5: A) Cu; B) Cd and C) Pb. Symbols represent experimental data,
750 and lines represent the Langmuir-Freundlich isotherm fits.

Graphical Abstract

Air pollution biomonitors - transplanted mosses

terrestrial

S. palustre* vs. *P. purum* vs. *F. antipyretica

aquatic

Field exposures

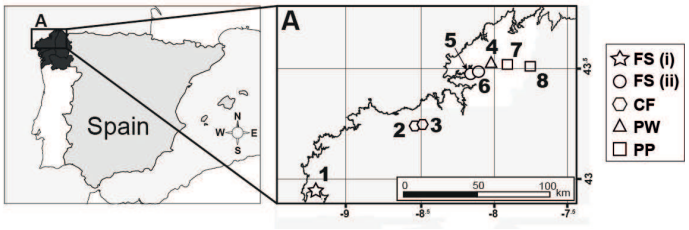

Higher trace metal uptake in *S. palustre* except for Hg (higher in *F. antipyretica*)

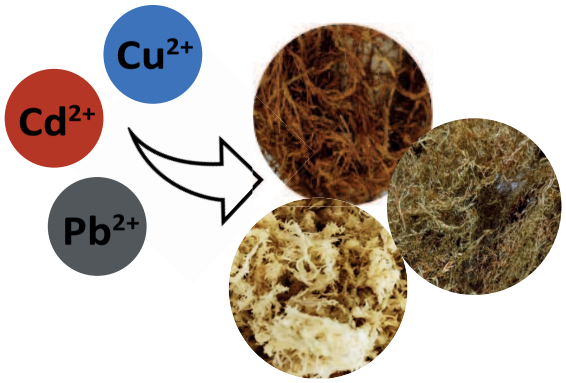

Laboratory experiments

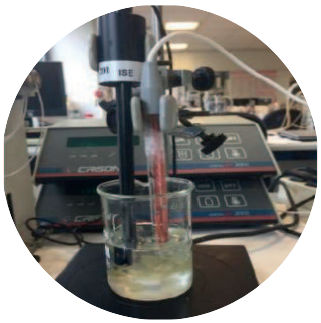

Similar nature of functional groups in the three moss species

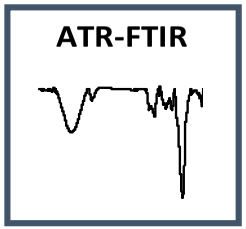

Higher concentration of acidic functional groups in terrestrial species

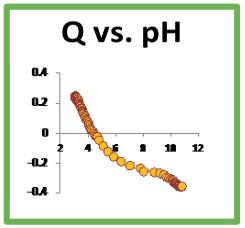

S. palustre the most efficient adsorbent of metal cations

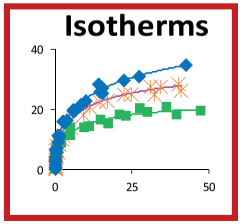

Figure 1

Click here to access/download;Figure;Fig. 1.eps

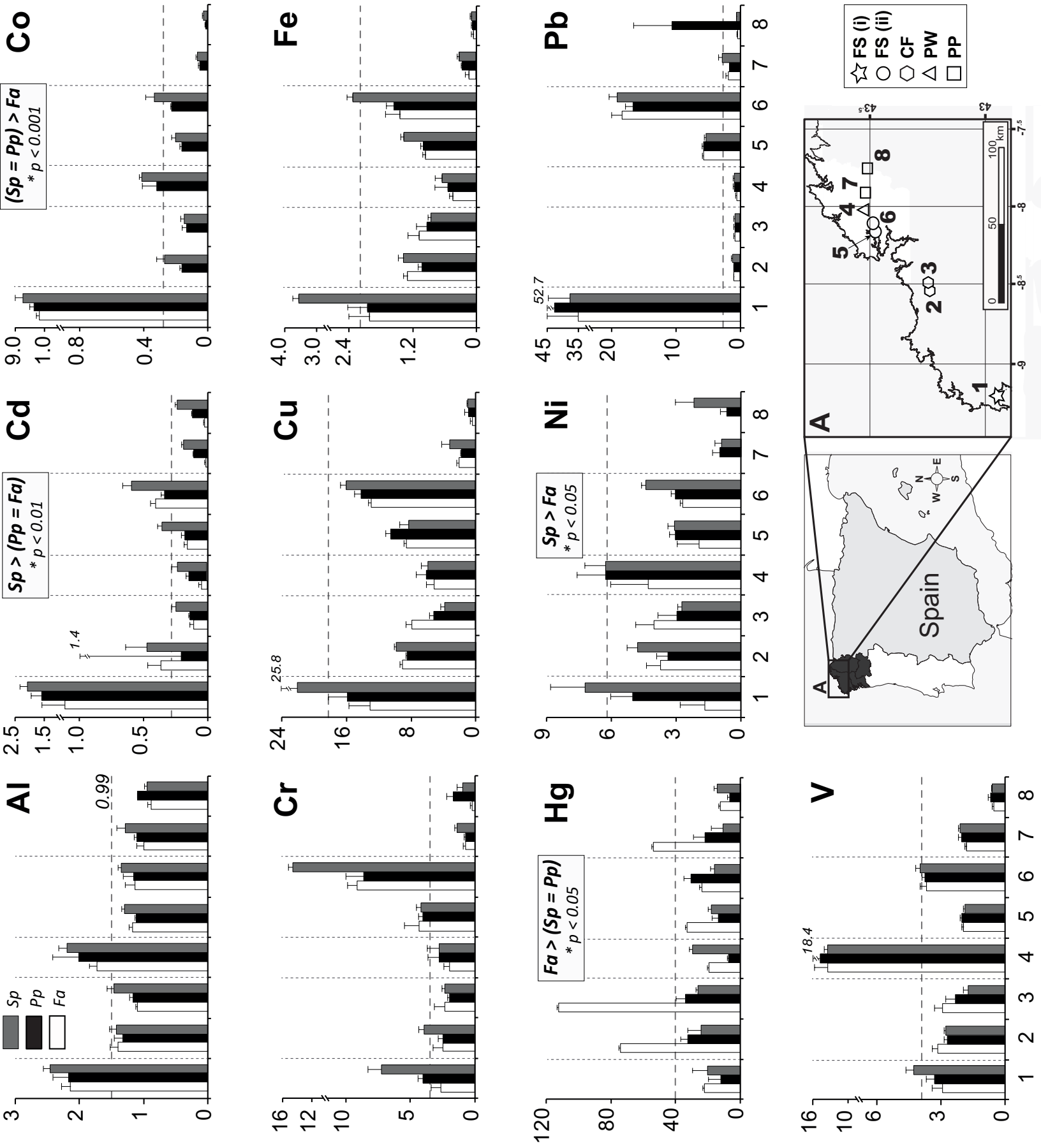

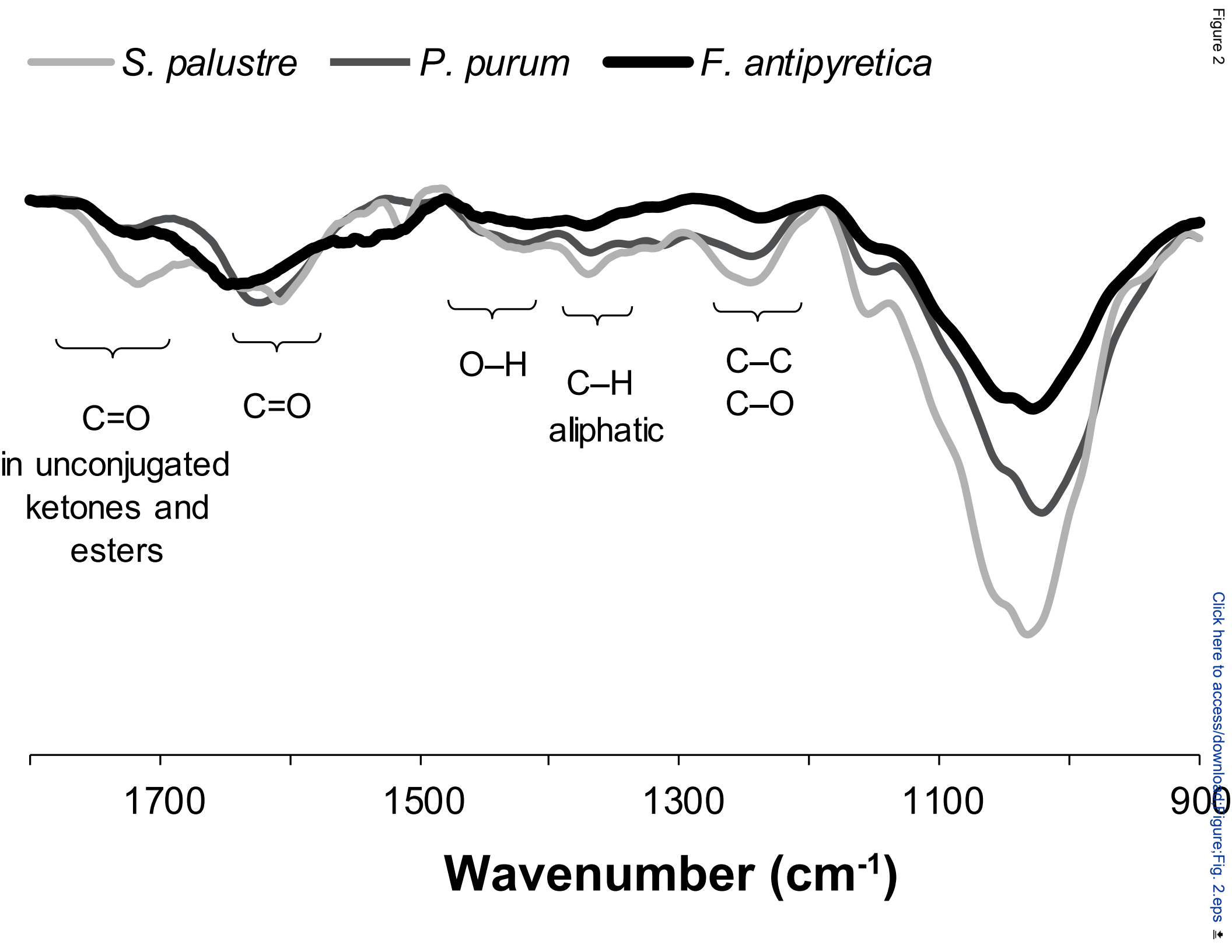

Figure 3

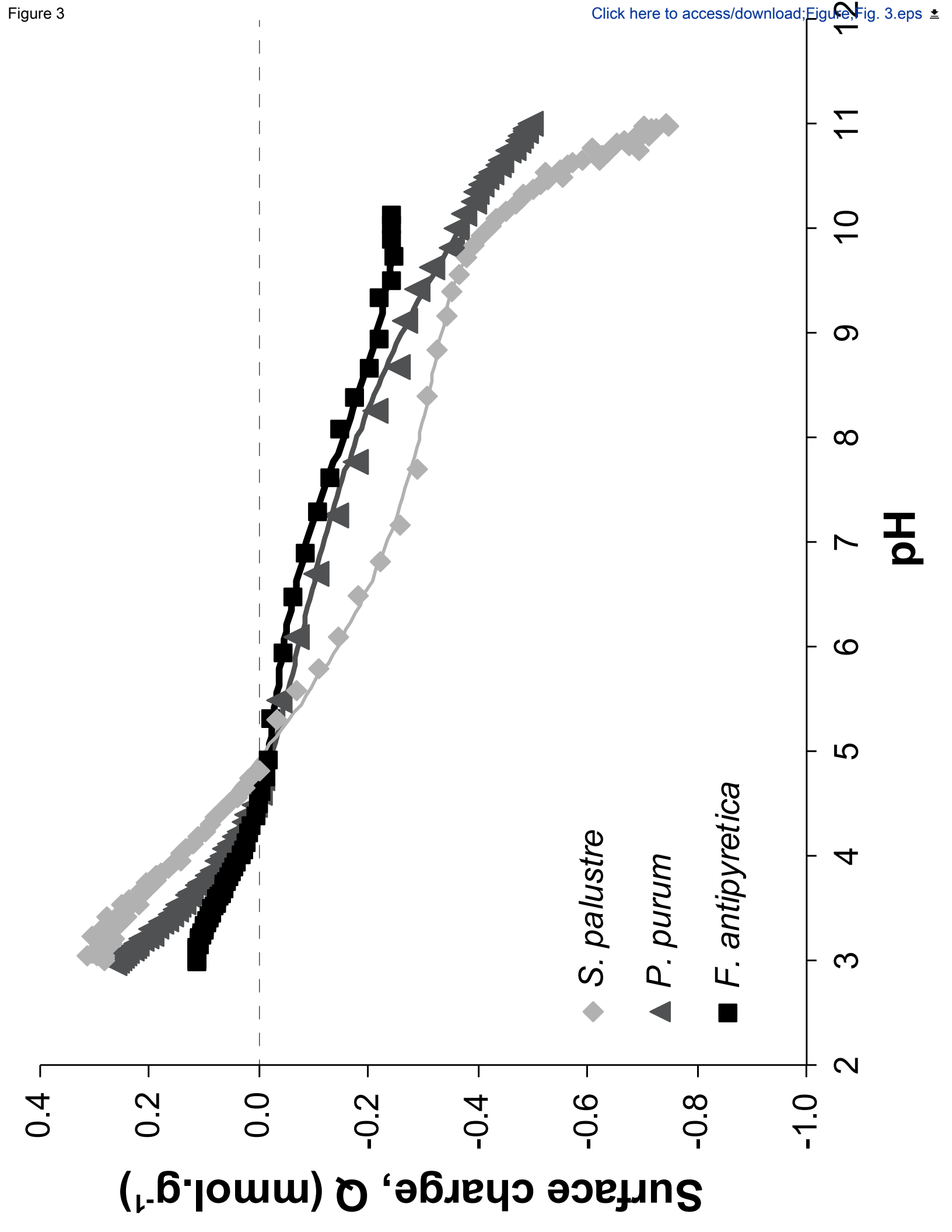

Figure 4

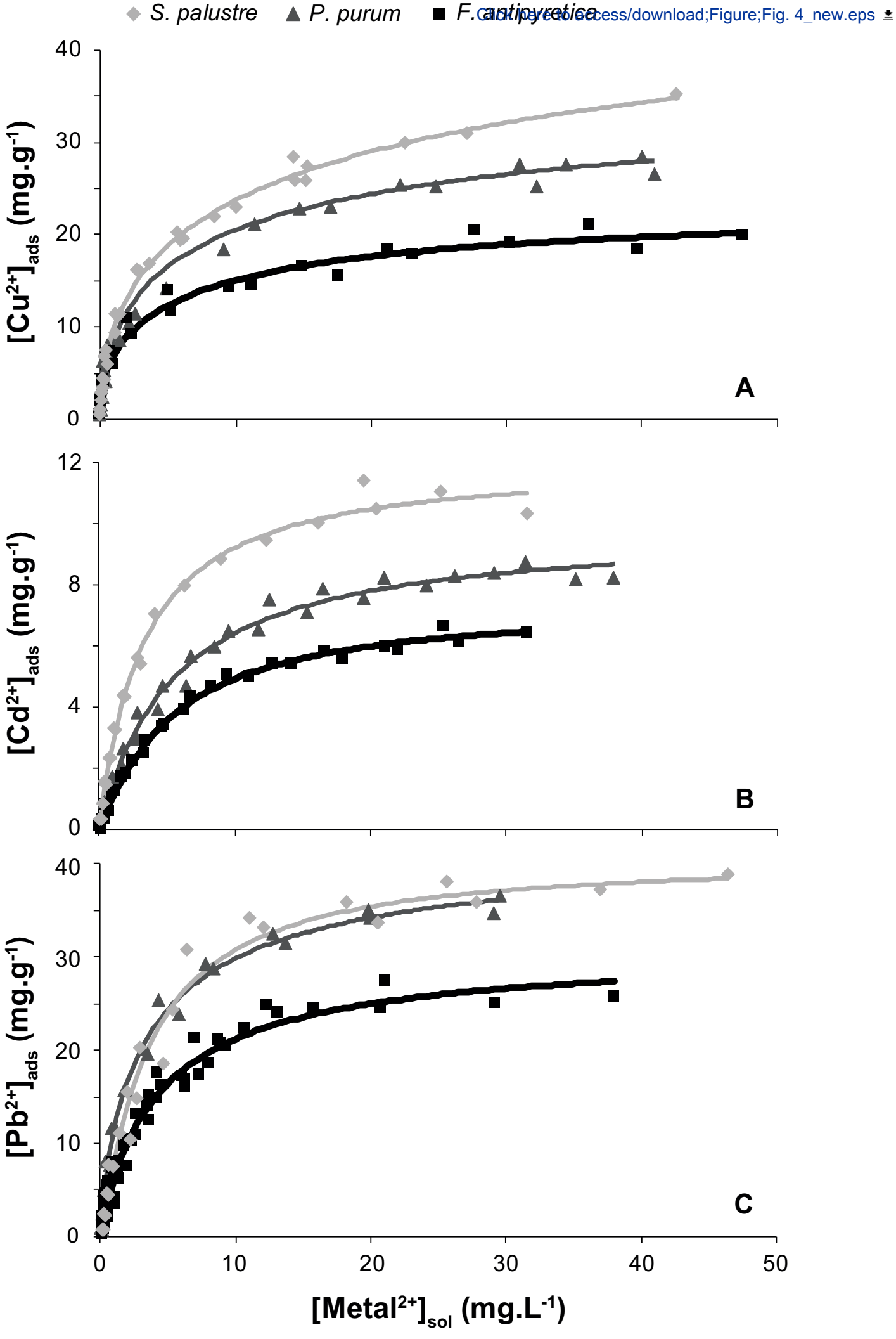
S. palustre
P. purum
F. antipyretica
[Cu2+]ads (mg.g-1)
[Cd2+]ads (mg.g-1)
[Pb2+]ads (mg.g-1)
[Metal2+]sol (mg.L-1)
A
B
C
0
10
20
30
40
4
8
12
50

726 **Tables**

727 **Table 1.** Comparison of some characteristic wavenumbers of the *Fontinalis antipyretica*
728 ATR–FTIR spectra before and after Cu^{2+} or Cd^{2+} adsorption. Shift–Me indicates the shift
729 in wavenumber before and after Cu^{2+} or Cd^{2+} adsorption; Δ(Cu–Cd) shift represents the
730 difference between the shifts in the wavenumbers observed after Cu and Cd adsorption.

731

Wavenumber (cm^{-1})						Assignation
Before adsorption	**After Cu adsorption**	**After Cd adsorption**	**Shift–Cu**	**Shift–Cd**	**Δ(Cu–Cd) shift**	
3344	3334	3334	10	10	0	O-H, N-H
2922	2920	2924	2	− 2	− 4	C-H in CH_3 and CH_2
1543	1542	1539	1	4	3	C=O
1372	1372	1373	0	− 1	− 1	Aliphatic C-H
1239	1243	1243	− 4	− 4	0	C-C and C-O
1028	1025	1025	3	3	0	O-H, C-O in secondary alcohols and ethers

732

733 **Table 2**. Acid-base fitting parameters of the 2-position Langmuir-Freundlich model for

734 *Sphagnum palustre, Pseudoscleropodium purum* and *Fontinalis antipyretica*. d.w.: dry weight.

735

	S. palustre	***P. purum***	***F. antipyretica***
$log\ K_1$	3.97	2.67	3.72
$log\ K_2$	11.08	10.98	7.86
S_1 (mmol g^{-1} d.w.)	1.04	0.75	0.16
S_2 (mmol g^{-1} d.w.)	0.89	0.93	0.25
m_1	0.28	0.57	0.95
m_2	0.98	0.23	0.48
R^2	0.998	0.999	0.998
RMSE	0.019	0.002	8x10-4

736

737 **Table 3**. Langmuir-Freundlich fitting parameters for the adsorption of Cu, Cd and Pb by

738 *Sphagnum palustre, Pseudoscleropodium purum* and *Fontinalis antipyretica*.

739

		S. palustre	***P. purum***	***F. antipyretica***
Cu	$log\ K_{LF}$	0.12	0.20	0.05
	Q_{max} (mg g^{-1})	45.2	34.6	23.1
	n	1.64	1.55	2.58
	R^2	0.99	0.98	0.98
	RMSE	26.9	48.02	21.1
Cd	$log\ K_{LF}$	0.31	0.18	0.19
	Q_{max} (mg g^{-1})	12.1	9.87	7.39
	n	1.04	1.02	1.10
	R^2	0.99	0.99	0.99
	RMSE	2.178	2.659	0.641
Pb	$log\ K_{LF}$	0.28	0.29	0.23
	Q_{max} (mg g^{-1})	40.7	42.7	31.0
	n	1.11	0.80	0.94
	R^2	0.98	0.99	0.97
	RMSE	102.2	34.5	113.2

740